

# Fourier-transform method of phase-shift determination

Kenneth A. Goldberg and Jeffrey Bokor

A new phase-shifting interferometry analysis technique has been developed to overcome the errors introduced by nonlinear, irregular, or unknown phase-step increments. In the presence of a spatial carrier frequency, by observation of the phase of the first-order maximum in the Fourier domain, the global phase-step positions can be measured, phase-shifting elements can be calibrated, and the accuracy of phase-shifting analysis can be improved. Furthermore, reliance on the calibration accuracy of transducers used in phase-shifting interferometry can be reduced; and phase-retrieval errors (e.g., fringe print-through) introduced by uncalibrated fluctuations in the phase-shifting phase increments can be alleviated. The method operates deterministically and does not rely on iterative global error minimization. Relative to other techniques, the number of recorded interferograms required for analysis can be reduced. © 2001 Optical Society of America

OCIS codes: 100.5070, 120.2650, 120.3180, 120.5050.

## 1. Introduction

The quest for high-accuracy wave-front-measuring interferometry techniques has given rise to a wide variety of data collection and analysis methods. Ranking high among them, phase-shifting interferometry has achieved widespread use in a variety of interferometric applications since its introduction three decades ago.<sup>1-4</sup> Recording interferometric data in the temporal domain, while a controlled, relative global phase shift is introduced between interfering beams, permits the phase at each point in the measurement domain to be calculated to within a multiple of  $2\pi$ . When the discrete temporal phase increments are known *a priori*, calculation is typically performed by the algebraic combination of separately measured intensities with different weights in a way that allows the stationary intensity, the modulated intensity, and the relative phase to be solved separately for each point.

The time-domain phase-shifting techniques offer several advantages over spatial-domain methods of interferogram analysis: improved noise immunity,

insensitivity to spatial variations in the detector response, high-spatial-frequency resolution, and ease of implementation. Ingenuity has produced a great variety of phase-retrieval algorithms to reduce susceptibility to systematic and random error sources.

General techniques have been developed to accommodate regular, irregular, and arbitrary step increments. A primary source of systematic error facing the early phase-retrieval methods came from the requirement that the phase steps be uniform and well characterized. Error minimization for linear phase-shift miscalibration has been addressed by several authors.<sup>5-12</sup> A  $j + 3$  sample algorithm that eliminates the effects of linear phase-shift miscalibration and harmonic components of the signal up to the  $j$ th order was developed by Larkin and Oreb.<sup>7</sup> Schmidt and Creath<sup>13</sup> proposed several algorithms for compensating phase shifts with quadratic nonlinearity, and de Groot developed a method to address cubic nonlinearity.<sup>14</sup> The susceptibility of phase-recovery techniques to random phase-shift errors has also been addressed,<sup>5,15</sup> and methods to reduce measurement errors have been proposed.<sup>16</sup> Paradoxically, error-compensating algorithms developed specifically to reduce susceptibility to systematic errors are generally more susceptible to random noise.<sup>15-18</sup> For this reason, techniques have been proposed to minimize the susceptibility to both systematic and random noise simultaneously.<sup>16</sup>

It is evident from a survey of the literature that much of the effort in the development of phase-shifting techniques has been spent addressing errors introduced by the phase-shifting itself. A different

---

The authors are with the Center for X-Ray Optics, Lawrence Berkeley National Laboratory, 1 Cyclotron Road, Mail Stop 2-400, Berkeley, California 94720-0001. The e-mail address for K. A. Goldberg is kagoldberg@lbl.gov. J. Bokor is also with the Department of Electrical Engineering and Computer Sciences, University of California, Berkeley, Berkeley, California 94720.

Received 19 October 2000; revised manuscript received 27 February 2001.

0003-6935/01/172886-09\$15.00/0

© 2001 Optical Society of America

approach, which has led to a separate class of phase-retrieval algorithms, measures the individual phase-step values during the phase recovery and uses that information to eliminate the measurement errors introduced by phase-step miscalibrations, nonlinearities, and random step errors. Methods have been developed to determine simultaneously both the global phase increment and the unknown relative phase at each point. Authors Kinnstaetter *et al.*,<sup>19</sup> and later Han and Kim,<sup>20</sup> and Kim *et al.*<sup>21</sup> have developed iterative techniques to reduce a global error function that incorporates the global phase steps as global-free parameters. Statistical approaches that exploit the nonlinear response of the phase-retrieval algorithms have been described by Dobroiu *et al.*<sup>22,23</sup>: These procedures also rely on iteration. The compound problem of translational and tilt-shift errors during phase shifting has been addressed with an iterative solution by Chen *et al.*<sup>24</sup>

The method described here falls into this latter category but operates deterministically by examining the Fourier domain without the necessity of iterative error minimization. By measuring and using the actual phase-step positions during the phase retrieval, we eliminate the need to suppress the temporal harmonic artifacts that cause fringe print-through, and the number of interferograms necessary to achieve arbitrary accuracy can be reduced. Because the method measures the experimental phase steps, it can also be used to study and calibrate the behavior of phase-shifting elements. Because no iteration is required, the method can be designed to operate rapidly.

In this paper we present a demonstration of this method applied to data from an extreme ultraviolet (EUV) phase-shifting point-diffraction interferometer (PSPDI).

## 2. Addressing Phase-Step Uncertainty

When a finite number of interferograms are recorded, with a global relative phase increment between each, and all other experimental parameters are held constant during the exposure series, then a convenient general representation of the  $n$ th interference pattern is

$$I_n(\mathbf{r}) = A(\mathbf{r}) + B(\mathbf{r})\cos[\phi(\mathbf{r}) + \Delta_n]. \quad (1)$$

The integer  $n$  can be regarded as the temporal-domain index of the individual steps. Here  $\mathbf{r}$  is a spatial coordinate spanning the measurement domain,  $A(\mathbf{r})$  is the stationary intensity,  $B(\mathbf{r})$  is the modulated intensity,  $\{\Delta_n\}$  is the set of  $N$  global phase-shift values, and  $\phi(\mathbf{r})$  is the relative phase we seek. When  $N \geq 3$  interferograms are recorded, and  $\{\Delta_n\}$  are known *a priori*, the system of  $N$  equations and three unknowns is, in principle, analytically solvable at each individual point in the domain. However, if the  $N$  global phase values  $\{\Delta_n\}$  are not known, then the solution involves  $N$  equations and  $N + 2$  unknowns. (If we allow  $\phi(\mathbf{r})$  to include an arbitrary constant offset,  $\Delta_0$  can always be defined as identi-

cally zero, reducing the number of unknowns by one, without loss of generality.)

### A. Methods of Accommodating Phase-Step Miscalibrations

To accommodate first-order miscalibrations in the global phase increment,  $\{\Delta_n\}$  can be modeled with an unknown linear step as  $\Delta_n = \alpha n$ . With four unknowns at each domain point ( $A$ ,  $B$ ,  $\phi$ , and  $\alpha$ ), the system is analytically solvable when four or more interferograms are recorded. Unknown phase-increment nonlinearities can be addressed in a similar fashion with the insertion of additional polynomial parameters in the expression for  $\Delta_n$ , combined with the recording of additional interferograms: one additional interferogram is required for each additional polynomial order in the expression for  $\Delta_n$ . By induction, the minimum number of required interferograms  $N$  will always equal three plus the number of free parameters in the description of  $\Delta_n$ .

Difficulty in this form of analysis arises when the global phase increments are irregular or unknown. The representation of  $N$  arbitrary global phase increments requires a polynomial of order  $N - 1$  in  $n$ . This number of free parameters precludes us from finding an analytic solution for the  $N + 2$  unknowns given only  $N$  interferograms. When an independent solution is sought for each separate domain point, the latter statement is true. However, if we assume that all of the domain points experience the same global phase increments, the information necessary for a full solution is available if we modify our approach.

### B. Different Approach: Measuring the Global Phase-Shift Positions

A separate class of phase-shifting phase-recovery methods treats each of the  $N$  phase steps as a free parameter and seeks to minimize a global error function that includes the unknown phase-shift positions and the unknown phase at each point. Here an iterative approach is applied to the error function minimization.<sup>20,21</sup> The free parameters now include the  $N - 1$  phase increments plus the stationary and modulated intensities and the phase at each point. If the initial guesses are close to the actual phase increments, then a satisfactory solution can be found within a few iterations. However, for unknown phase increments, the high degree of interdependence among the free parameters of the fit, the nonlinear dependence of the global error function on the phase-step values, and the built-in degeneracy caused by the excess of free parameters versus the number of interferograms can introduce computational difficulties. It may be difficult to assess whether a given solution represents a local or a global minimum of the error function; this issue is compounded by the interdependence of the phase-step parameters. In addition, such techniques may be highly sensitive to source intensity fluctuations within the interferogram data series.

The phase-retrieval method described in this paper is divided into two steps performed in sequence. First, the  $N$  global phase positions are determined by Fourier-domain analysis; this is called the Fourier-transform phase-shift determination (FTPSD) method. The phase positions are then applied as *a priori* information to the least-squares method (LSM) of phase retrieval.<sup>3,25,26</sup> Application of this method requires the presence of a spatial carrier frequency, or wave-front tilt, in the measurement domain. This matches the requirements necessary for the application of the Fourier-transform methods of interferogram analysis: Given the point-spread function of the optical system under test, the spatial carrier frequency must be high enough to adequately separate the first-order signal from the zeroth-order components in the Fourier domain.<sup>27</sup> If this requirement is not satisfied over the full domain of measurement (because of high fringe curvature or insufficient tilt), the method can be applied on a subdomain over which the conditions are met. Because the phase-shift positions we seek are global, the FTPSD method does not suffer significantly when performed on a subdomain. Such a subdomain can be any appropriate subset of the interferogram data, including a nonsquare or nonrectangular region, or a single line of data.

With the FTPSD method, no *a priori* information about the phase steps and no initial-guess values are required. As long as the phase-shift values do not comprise a degenerate set (i.e., the values are unique), the phase steps can be of any magnitude, take any values, and be computed in any order. This method finds the phase steps deterministically, not iteratively; there are no concerns with achieving convergence.

### 3. Solution of the Global Phase Positions with the Fourier-Transform Phase-Shift Determination Method

Following the derivation of the widely known Fourier-transform method of interferogram analysis,<sup>27-29</sup> in the presence of a spatial carrier frequency  $\mathbf{k}_0$ , the piston (constant) and tilt (linear phase) terms can be separated from the phase function of interest. We define  $\phi(\mathbf{r})$  to include the tilt as

$$\phi(\mathbf{r}) \equiv \phi_0(\mathbf{r}) + \mathbf{k}_0 \cdot \mathbf{r}. \quad (2)$$

Equation (1) then becomes

$$I_n(\mathbf{r}) = A(\mathbf{r}) + B(\mathbf{r})\cos[\phi_0(\mathbf{r}) + \mathbf{k}_0 \cdot \mathbf{r} + \Delta_n]. \quad (3)$$

By definition, across the measurement domain (or a subdomain used for this calculation)  $\phi_0(\mathbf{r})$  contains no net piston or tilt components.

To facilitate Fourier-domain analysis, the constant and the tilt terms are separated from the cosine argument, and we expand the expression as

$$I_n(\mathbf{r}) = A(\mathbf{r}) + \exp(i\Delta_n)C(\mathbf{r})\exp(i\mathbf{k}_0 \cdot \mathbf{r}) + \exp(-i\Delta_n)C^*(\mathbf{r})\exp(-i\mathbf{k}_0 \cdot \mathbf{r}), \quad (4)$$

using the definition

$$C(\mathbf{r}) \equiv \frac{1}{2}B(\mathbf{r})\exp[i\phi_0(\mathbf{r})], \quad (5)$$

where  $*$  indicates the complex conjugate.

The Fourier transform of  $I_n(\mathbf{r})$  is  $i_n(\mathbf{k})$ , given by

$$i_n(\mathbf{k}) = a(\mathbf{k}) + \exp(i\Delta_n)c(\mathbf{k} - \mathbf{k}_0) + \exp(-i\Delta_n)c^*(\mathbf{k} + \mathbf{k}_0), \quad (6)$$

with  $a(\mathbf{k})$  and  $c(\mathbf{k})$  being the Fourier transforms of  $A(\mathbf{r})$  and  $C(\mathbf{r})$ , respectively. Typically dominated by low-spatial-frequency components,  $a(\mathbf{k})$  and  $c(\mathbf{k})$  are both strongly peaked at the zero frequency. Displacement of  $c(\mathbf{k})$  by  $\pm\mathbf{k}_0$  separates the modulated from the stationary intensity components.

The presence of  $\exp(i\Delta_n)$  as a coefficient of  $c(\mathbf{k} - \mathbf{k}_0)$  allows us to isolate the global phase positions  $\{\Delta_n\}$  by examining the complex phase of the Fourier transform at  $\mathbf{k}_0$  where  $c(\mathbf{k} - \mathbf{k}_0)$  is maximum:

$$i_n(\mathbf{k}_0) = a(\mathbf{k}_0) + \exp(i\Delta_n)c(0) + \exp(-i\Delta_n)c^*(2\mathbf{k}_0) \quad (7a)$$

$$\approx \exp(i\Delta_n)c(0), \quad (7b)$$

where  $c(0)$  is a complex constant. Therefore, apart from a constant phase offset,

$$\Delta_n \approx \tan^{-1}[i_n(\mathbf{k}_0)], \text{ or } \Delta_n \approx \text{Im}\{\ln[i_n(\mathbf{k}_0)]\}. \quad (8)$$

The additional additive phase angle determined by the complex constant  $c(0)$  is the same for each interferogram and is thus absorbed into the piston term in the analysis. Calculation of the individual phase-step values requires only that the Fourier transform be calculated at one point, the spatial carrier frequency  $\mathbf{k}_0$ . (This fact can be used to significantly reduce computation times in circumstances in which  $\mathbf{k}_0$  is known in advance. Assumed constant within a measurement series,  $\mathbf{k}_0$  need be measured only once.)

Successful application of this method relies on the Fourier-domain separability of the three terms of Eq. (6), as determined by the spatial-frequency content of each. The quality of the approximation (i.e., the uncertainty in the measurement) depends on the relative magnitudes of  $c(0)$ ,  $a(\mathbf{k}_0)$ , and  $c(2\mathbf{k}_0)$ , the additive constituents of  $i_n(\mathbf{k}_0)$ . In practice, because  $a(\mathbf{k})$  and  $c(\mathbf{k})$  may span the spatial-frequency spectrum, care must be taken to ensure adequate separation of the orders in the spatial-frequency domain of measurement. This requirement is also true whenever the Fourier-transform methods of interferogram analysis are applied.

Determination of the global phase-step values does not require use of the entire interferogram in the calculations. In the presence of closed fringes, large variation in the fringe density across the measurement domain, or regions of poor signal-to-noise ratio, a subdomain of the data that satisfies the above requirements can be chosen. By assumption, the global phase increments introduce the same relative phase shift to all points in the domain equally; therefore use of an appropriate subdomain of the data is

not problematic. When a subdomain is used, the spatial carrier frequency of interest becomes that corresponding to the subdomain only.

#### A. Determination of the Spatial Carrier Frequency

When the spatial carrier frequency  $\mathbf{k}_0$  is unknown, there are several methods of varying the complexity available to determine it. One simple method is to identify the position of peak magnitude in the Fourier domain, in an area that excludes the central-frequency components. Use of the fast Fourier transform of an interferogram from the phase-shifting series (or a subdomain of an interferogram) is one straightforward way to implement this search. Because of the discretization of the fast Fourier-transform domain, the uncertainty in the location of  $\mathbf{k}_0$  by this method alone is one-half cycle.

An alternative and more accurate method calculates the spatial carrier frequency from the tilt in a measured interferogram (or subdomain). Here the Fourier-transform method of interferogram analysis is applied to a single interferogram or subdomain, thus recovering the wave-front phase across the domain. This wave front can be calculated coarsely, with or without strong filtering in the spatial-frequency domain because only the tilt component is of interest. Filtering may also simplify the unwrapping procedure that accompanies phase retrieval with the Fourier-transform method. The spatial carrier frequency we seek is proportional to the two-dimensional ( $x$  and  $y$ ) tilt component of the measured wave-front phase.

#### B. Evaluation of $\Delta_n$

Once the spatial carrier frequency is known (and it is assumed to be the same for each of the interferograms in a phase-shifting series), then phase-step determination proceeds by the calculation of the Fourier transform at  $\mathbf{k}_0$ ,  $i_n(\mathbf{k}_0)$ . Because there is only one point of interest in the Fourier domain, an expedient discreet calculation that approximates the integral,

$$i_n(\mathbf{k}_0) = \int I_n(\mathbf{r}) \exp(i\mathbf{k}_0 \cdot \mathbf{r}) d\mathbf{r}, \quad (9)$$

is all that is required. Substituting Eq. (9) into approximations (8) allows us to state the method more succinctly:

$$\Delta_n \approx \tan^{-1} \left[ \int I_n(\mathbf{r}) \exp(i\mathbf{k}_0 \cdot \mathbf{r}) d\mathbf{r} \right]. \quad (10)$$

With the global-phase positions  $\{\Delta_n\}$  now solvable from the interferograms of a series, these values can be treated as *a priori* information in the application of conventional phase-shifting techniques to recover the phase at each point in the measurement domain. The LSM is a well-suited candidate method that accommodates arbitrary phase values and incorporates additional error minimization. The LSM is discussed in detail in Appendix A.

#### C. Error Estimation

The uncertainty in phase-shift determination by use of the spatial-frequency domain depends primarily on the relative amplitudes of the functions  $c(\mathbf{k} - \mathbf{k}_0)$ ,  $c^*(\mathbf{k} + \mathbf{k}_0)$ , and  $a(\mathbf{k})$ , near  $\mathbf{k} = \mathbf{k}_0$ . These amplitudes determine the validity of approximation (7b). The phase of interest  $\Delta_n$  is found in the coefficient of  $c(0)$  in Eq. (7a) and is given by approximations (8). The error magnitude in these approximations cannot be determined while  $c(\mathbf{k})$  and  $a(\mathbf{k})$  are unknown. However, when we examine the behavior of the Fourier-transform components at  $\mathbf{k}_0$  within a phase-shifting series of interferograms, an estimate of the error magnitude is easily made.

For an individual phase step, the three quantities  $c(0)$ ,  $c^*(2\mathbf{k}_0)$ , and  $a(\mathbf{k}_0)$  and the  $\Delta_n$ -dependent complex coefficients found in Eq. (7a) can be regarded as complex scalars, or vectors in the complex plane. If we assume that all other experimental conditions are held fixed while the phase-shifting series is recorded, only the unit-magnitude coefficients of  $c(\mathbf{k} - \mathbf{k}_0)$  and  $c^*(\mathbf{k} + \mathbf{k}_0)$  are affected. To separate the one term of interest from the other two, we define two complex constants  $p$  and  $q$ :

$$p \equiv \exp(i\Delta_n)c(0), \quad (11a)$$

$$q \equiv a(\mathbf{k}_0) + \exp(-i\Delta_n)c^*(2\mathbf{k}_0), \quad (11b)$$

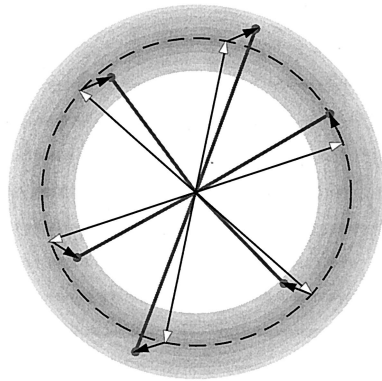
$$i_n(\mathbf{k}_0) = p + q, \quad (11c)$$

where  $p$  represents the phase of the sidelobe peak that contains the phase we seek and  $q$  is the magnitude of the additional components that here contribute to the uncertainty. In most experimental situations of interest, it is safe to assume that  $p \gg q$  and that the phases of  $p$  and  $q$  are independent. Within the phase-shifting series, the relative phases of the three components of Eq. (7a) are correlated, related to each other by factors of  $\exp(i\Delta_n)$ .

Figure 1 shows a representation of  $p$  for six  $60^\circ$  phase steps in the complex plane. Only the resultant vectors are measurable. The largest phase error [between  $p$  and the measured value of  $i(\mathbf{k}_0)$ ] occurs when  $q$  is perpendicular to  $p$ . When  $q$  is significantly smaller than  $p$ , the magnitude of the maximum error in the measured phase  $\delta\Delta_n$  is approximately

$$\delta\Delta_n \approx |q|/|p|. \quad (12)$$

Because  $\delta\Delta_n$  depends on the ratio of  $|q|$  to  $|p|$ , we can achieve error minimization in two ways: increasing  $|p|$  or reducing  $|q|$ .  $|p|$  is increased when we ensure that the calculated carrier frequency occurs at the peak value of the spatial-frequency-domain sidelobe  $c(\mathbf{k} - \mathbf{k}_0)$ .  $|q|$  depends on the spatial-frequency content of  $c^*(\mathbf{k})$  and  $a(\mathbf{k})$ . In general, it can be reduced only when the spatial carrier frequency is increased so as to reduce the overlap of the orders in the Fourier domain. Improvements in the fringe contrast reduce the relative magnitude of  $a(\mathbf{k})$  and also improve the ratio of  $|q|$  to  $|p|$ .



$\longrightarrow$ :  $\exp(i\Delta_n) c(0)$   
 $\uparrow$ :  $a(\mathbf{k}_0) + \exp(-i\Delta_n) c^*(2\mathbf{k}_0)$   
 $\longrightarrow \bullet$ :  $i_n(\mathbf{k}_0)$  resultant

$$\begin{aligned}
 i_n(\mathbf{k}_0) &= a(\mathbf{k}_0) + \exp(i\Delta_n) c(0) + \exp(-i\Delta_n) c^*(2\mathbf{k}_0) \\
 &\approx \exp(i\Delta_n) c(0)
 \end{aligned}$$

Fig. 1. Complex-plane phasor representation of the spatial carrier frequency peak of the Fourier transform of six hypothetical interferograms. The resultant, measured amplitude (indicated by the gray line segments with small filled circles) is the sum of three terms, as described by Eq. 7(a): The largest term is the first-order peak. It is the phase of this term in each measurement of the series that reveals the phase-step values we seek.

Experimentally, the relative magnitudes of  $q$  and  $p$ , and hence the phase uncertainty  $\delta\Delta_n$ , can be estimated from the data. The variation in the measured magnitude of  $i_n(\mathbf{k}_0)$  is related to the magnitudes of  $q$  and  $p$ . The magnitude  $|i_n(\mathbf{k}_0)|$  varies between the minimum and the maximum values of  $|p - q|$ . The maximum and minimum occur when  $p$  and  $q$  are in phase or are  $180^\circ$  out of phase, respectively. We define  $M_0 = \min\{|i_n(\mathbf{k}_0)|\}$  and  $M_1 = \max\{|i_n(\mathbf{k}_0)|\}$  for the measured data:

$$|q| > \frac{1}{2}(M_1 - M_0). \quad (13)$$

A limitation of this estimation is that, for a small sampling of phase-shift values, there is no guarantee that the maximum and minimum possible values of  $i_n(\mathbf{k}_0)$  will be observed. Additional measurements improve the estimation.

When Eqs. (11) and inequality (12) are combined, the estimated measurement uncertainty in any given phase step is bounded by

$$\delta\Delta_n \leq \frac{M_1 - M_0}{M_1 + M_0}. \quad (14)$$

Once the phase-step uncertainty is known, the uncertainty in the measured phase at each point can be calculated; it is dependent on the phase-shifting analysis algorithm that is used. The error propagation calculation is equivalent to the analysis of the rela-

tionship between phase-step errors and the rms error in the measured phase at each point. Brophy<sup>17</sup> and Hibino<sup>16</sup> have shown that, for small random step errors with a Gaussian error distribution, the rms wave-front phase error is proportional to the rms phase-step error magnitude, and it typically decreases with the number  $N$  of interferograms by  $N^{-1/2}$ . This analysis applies to the present situation in which the random error occurs in the phase-step determination rather than the phase-step implementation.

#### 4. Experimental Demonstration

The point-by-point accuracy of wave-front measurements can be improved by the application of the FTPSD method. The degree of improvement depends on the rms magnitude of the phase-step errors in the measurement, the uncertainty in the phase-step determination, and on the specific phase-shifting analysis algorithm applied to recover the wave front. These properties are case specific and may vary even from one measurement to the next. The following example illustrates the operation and benefits of the FTPSD method.

The FTPSD method is now part of the routine data analysis procedure used with the EUV PSPDI operating at the Advanced Light Source at Lawrence Berkeley National Laboratory.<sup>30,31</sup> The optics under test are prototype multielement reflective systems operating at a 13.4-nm wavelength and designed for EUV lithography research.<sup>32</sup> Molybdenum silicon multilayer coatings provide the mirrors with over 65% reflectivity near normal incidence. These systems have demonstrated nearly diffraction-limited performance with low-frequency system wave-front quality in the half-nanometer rms range,<sup>33</sup> and the PSPDI has a measured accuracy as high as 0.04-nm rms within a numerical aperture (N.A.) of 0.081.<sup>31</sup>

The demonstration presented here comes from the wave-front measurement of an EUV 10 $\times$ -demagnification Schwarzschild objective. The optic is measured across an off-axis circular subaperture with a 0.088 N.A.; an EUV-sensitive CCD camera records the interference pattern. A square domain with 256  $\times$  256 measurement points, subtending 60% of the pupil's width, is used for this demonstration. The phase-shifting element is a transmission grating beam splitter that is translated in plane in the direction orthogonal to the grating lines. A spatial filter in the optic's image plane blocks all but the zeroth and the first diffracted order from the grating, so only two orders combine to produce the interference pattern. The measurements are performed in vacuum at a base pressure of  $10^{-7}$  Torr.

Ten interferograms are recorded with a phase shift performed between each step. A typical interferogram is shown in Fig. 2. Below the image is a cross section of the fringe pattern intensity. The target phase-shifting-step increment was set to one-quarter cycle. Application of the FTPSD method reveals the actual phase-step values through inspection of the

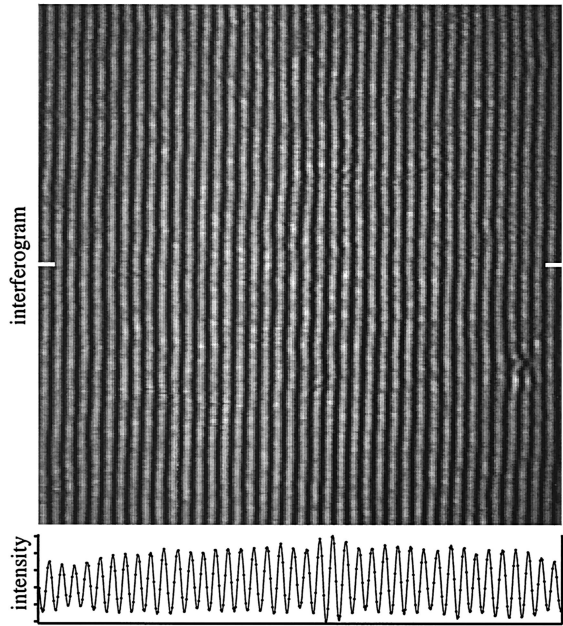


Fig. 2. Detail from a typical interferogram image from a phase-shifting series recorded with the EUV PSPDI. The test optic is a molybdenum silicon multilayer-coated Schwarzschild objective operating at a 13.4-nm wavelength. The detail subtends 60% of the full 0.088 N.A. Below the interferogram is an intensity cross section taken through the central portion of the interferogram, indicated by the white lines at the edges. The cross section shows the high fringe contrast.

complex amplitude of the interferograms' Fourier transforms at the spatial carrier frequency. The measured phase steps are shown in Figs. 3 and 4. Figure 3 gives a complex-plane phasor representation of the spatial carrier frequency Fourier-domain peak

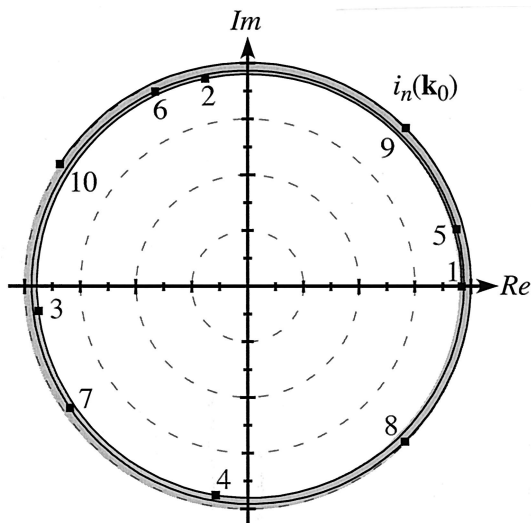


Fig. 3. Complex-plane phasor representation of the spatial carrier frequency Fourier-domain peak for a phase-shifting series of ten interferograms. Small amplitude fluctuations and a nonuniform step size can be seen. The phase-step values are calculated directly from the angle, and the uncertainty is estimated from the variation of the magnitude.

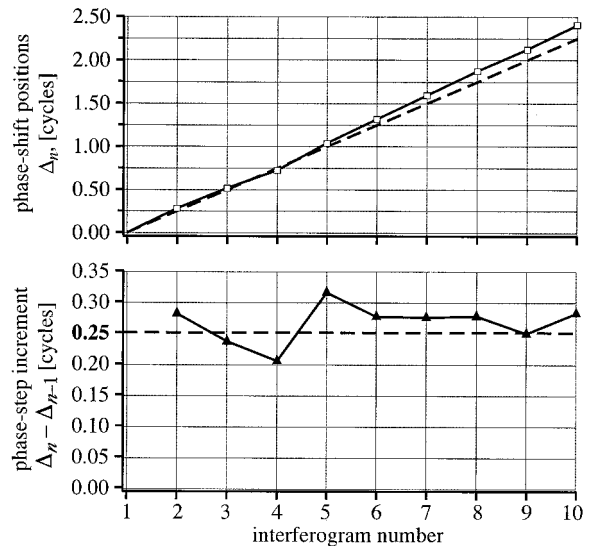


Fig. 4. (Top) Phase-step values and (Bottom) the step increments ( $\Delta_n - \Delta_{n-1}$ ) are shown for the phase-shifting series of ten interferograms. On both graphs the dashed lines indicate quarter-cycle phase steps.

in which the amplitude fluctuations discussed in Subsection 3.C can be observed. The phase steps are calculated directly from the angle, and the uncertainty is estimated from the variation of the magnitude. In Fig. 4 both the phase-step values and the step increments are shown. The uncertainty in the phase-step determination can be estimated by inequality (14): Its value is 0.0371 rad, 2.13 deg, or 2.36% of the target quarter-cycle phase-step increment.

To demonstrate the function of the FTPSD method, and its effectiveness with a limited number of input interferograms, the interferogram data were evaluated in two ways. The first four interferograms were analyzed with the FTPSD method to determine the phase-step values; this was followed by the LSM to determine the wave-front phase. Second, we recovered the wave-front phase from the first five interferograms using the Hariharan technique.<sup>34</sup> In both cases, the analysis reveals the wave-front phase across the measurement domain.

The wave-front phase maps shown in Fig. 5 reveal aberrations in the system wave front. The Hariharan technique is used to analyze the first five interferograms and generate the wave front  $\phi_1$  shown in Fig. 5(a). Fringe print-through at twice the fringe spatial frequency is visible in this data. The FTPSD method combined with the LSM is applied to the first four interferograms, and the resultant wave front  $\phi_2$  is shown in Fig. 5(b). In Fig. 5(c) the difference  $\phi_1 - \phi_2$  reveals strong fringe print-through at twice the fundamental fringe frequency, coming primarily from  $\phi_1$ . These two phase-map sections shown are taken from the central portion of the interferogram shown in Fig. 2.

Below the phase maps, phase cross sections taken through the center of the phase maps are shown (with

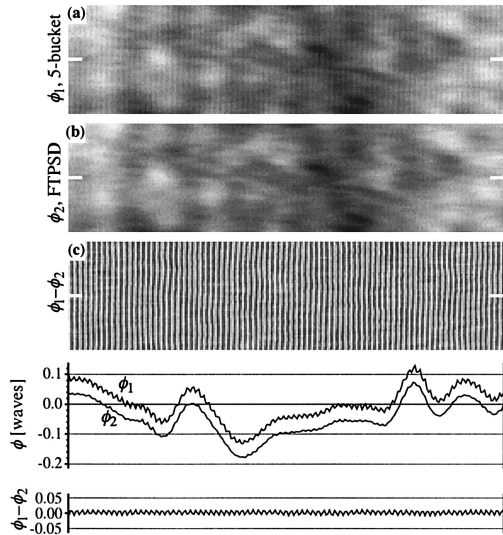


Fig. 5. Wave-front phase maps reveal aberrations in the system wave front. (a) First five interferograms analyzed with the Hariharan technique:  $\phi_1$ . (b) FTPSD method combined with the LSM, applied to the first four interferograms:  $\phi_2$ . Phase-map sections shown are taken from the center portion of the interferogram of Fig. 2; the gray scale is bounded on the range  $(-2.274$  to  $2.216$  nm). (c) The difference  $\phi_1 - \phi_2$  reveals strong fringe print-through at twice the fundamental fringe frequency, coming primarily from  $\phi_1$ . The difference is displayed on the gray-scale range  $(-0.180$  to  $0.139$  nm). Below (c) are cross sections of  $\phi_1$  and  $\phi_2$  plotted with a small constant displacement for clarity. Horizontal cross sections are taken from the central region of the wave-front data, indicated by horizontal lines at the edges. The difference  $\phi_1 - \phi_2$  is also shown. The rms magnitude of the difference wave front, attributable primarily to fringe print-through, is roughly 11% of the full-wave-front magnitudes.

a small phase displacement added for clarity), and their difference appears at the bottom of Fig. 5. Across the phase maps shown, the rms wave-front error magnitudes are nearly identical: 0.05710 waves (0.7651 nm) in the FTPSD and LSM case and 0.05719 waves (0.7663 nm) in the Hariharan case. However, the difference wave front has a rms magnitude of 0.00621 waves (0.08323 nm), roughly 11% of the full-wave-front magnitude. The difference is attributable primarily to the significant fringe print-through.

## 5. Conclusion

The method described here uses the complex phase of the spatial carrier frequency peak in the Fourier transform of an interferogram to deduce the global phase increments introduced during phase-shifting interferometry. Its importance grows with the magnitude of the uncertainty in the phase increments and with the demand for high-accuracy phase recovery. The method relies on the fact that the phase-shifting process affects only the constant phase component of the interference fringe pattern, leaving the spatially varying components of the optical path difference unchanged. By use of a large portion of the available interferometric data, without regard to the size and shape of the measurement domain, this

method can be extremely robust in the presence of noise, including intensity-level fluctuations, shot noise, and detector noise.

To be applicable, this method requires that the interferometric data satisfy the same criteria that apply to analysis with the widely known Fourier-domain techniques. Specifically, the carrier frequency peak must be separable from the central frequency in the Fourier spatial-frequency domain. When this condition is not met for an entire interferogram data set (because of closed fringes or other excluding factors), it can be met for a subregion of the data on which a nonzero carrier frequency can be identified. In such cases, the subregion then provides the global phase increment information for the entire interferogram.

In a further effort to improve the accuracy of the wave-front measurements in the EUV PSPDI, the FTPSD method is routinely applied in conjunction with the dual-domain analysis method.<sup>35</sup> The dual-domain method combines the spatial-filtering properties of the PSPDI with temporal-domain filtering from phase-shifting analysis to reduce the interferometer's susceptibility to noise from scattered light and other sources.

## Appendix A: Least-Squares Method of Phase-Shifting Analysis

The LSM<sup>3,25,26</sup> of phase-shifting analysis has been described by several authors. Because it is well suited for use in conjunction with the FTPSD method, a brief outline of the method is presented here. The LSM allows the reconstruction of wave-front data in phase-shifting interferometry when arbitrary global phase-shifting steps are known. As before, the  $N$  phase positions are defined as a set of  $N$  real values  $\{\Delta_n\}$ . The expression for the individual interferograms, Eq. (1), can be expanded into a new set of coefficients  $\{a_0, a_1, a_2\}$  as follows:

$$I_n(\mathbf{x}) = A(\mathbf{x}) + B(\mathbf{x})\cos[\phi(\mathbf{x}) + \Delta_n] \\ = a_0(\mathbf{x}) + a_1(\mathbf{x})\cos \Delta_n + a_2(\mathbf{x})\sin \Delta_n. \quad (\text{A1})$$

Here the phase steps  $\Delta_n$  were separated from the unknown phase  $\phi(x)$  by the definitions

$$a_0(\mathbf{x}) \equiv A(\mathbf{x}), \\ a_1(\mathbf{x}) \equiv B(\mathbf{x})\cos \phi(\mathbf{x}), \\ a_2(\mathbf{x}) \equiv -B(\mathbf{x})\sin \phi(\mathbf{x}). \quad (\text{A2})$$

These are the three unknowns for which we must solve. Because the phase steps are known *a priori*, the  $\sin \Delta_i$  and  $\cos \Delta_i$  terms are simply the scalar coefficients of the unknown  $a_1(x)$  and  $a_2(x)$  in Eqs. (11) and are identical for all points  $x$  in the measurement domain.

When we apply the method of least squares separately at each point  $x_i$  of  $\mathbf{x}$ , the goal is to minimize the

error function  $E^2(x_i)$ , defined as

$$E_i^2 \equiv E^2(x_i) \equiv \sum_{n=1}^N [I_n(x_i) - a_0(x_i) - a_1(x_i)\cos \Delta_n - a_2(x_i)\sin \Delta_n]^2. \quad (\text{A3})$$

The error function is related to the fit variance, where it is assumed that each measurement point  $I_i(x_i)$  contains the same uncertainty.

At each  $x_i$ , we minimize  $E^2(x_i)$  by differentiating Eq. (A3) with respect to the three unknowns  $a_0(x_i)$ ,  $a_1(x_i)$ , and  $a_2(x_i)$ . The resultant expression can be written in matrix form:

$$\begin{bmatrix} N & \Sigma \cos \Delta_n & \Sigma \sin \Delta_n \\ \Sigma \cos \Delta_n & \Sigma \cos^2 \Delta_n & \Sigma \cos \Delta_n \sin \Delta_n \\ \Sigma \sin \Delta_n & \Sigma \cos \Delta_n \sin \Delta_n & \Sigma \sin^2 \Delta_n \end{bmatrix} \times \begin{bmatrix} a_0(x_i) \\ a_1(x_i) \\ a_2(x_i) \end{bmatrix} = \begin{bmatrix} \Sigma I_n(x_i) \\ \Sigma I_n(x_i) \cos \Delta_n \\ \Sigma I_n(x_i) \sin \Delta_n \end{bmatrix}, \quad (\text{A4a})$$

$$\mathbf{A}(\Delta)\mathbf{a}(x_i) = \mathbf{b}(x_i, \Delta). \quad (\text{A4b})$$

Here  $\Sigma$  is a shorthand notation representing the sum over the  $N$  measurements, with  $n$  as the summation index. The symmetric matrix  $\mathbf{A}(\Delta)$ , called the curvature matrix, depends only on the known phase shifts, whereas the vector  $\mathbf{b}(x_i, \Delta)$  contains the measured interferogram data.  $\mathbf{A}(\Delta)$  can be calculated just once, yet the calculation of  $\mathbf{b}(x_i, \Delta)$  must be done separately at every point in the measurement domain. The solution for the coefficient vector  $\mathbf{a}(x_i)$  requires inverting  $\mathbf{A}(\Delta)$  and premultiplying both sides of Eq. (A4b):

$$\mathbf{a}(x_i) = \mathbf{A}^{-1}(\Delta)\mathbf{b}(x_i, \Delta). \quad (\text{A5})$$

When there are three or more unique phase steps, the rows will be independent and  $\mathbf{A}(\Delta)$  will be invertible. Once  $\mathbf{a}(x_i)$  is known, the phase  $\phi(x_i)$  and modulation  $\gamma(x_i)$  are easily found. Over the whole domain  $\mathbf{x}$ ,

$$\phi(\mathbf{x}) = \tan^{-1} \left[ \frac{-a_2(\mathbf{x})}{a_1(\mathbf{x})} \right], \text{ or} \\ \phi(\mathbf{x}) = \tan^{-1} [-a_2(\mathbf{x}), a_1(\mathbf{x})]. \quad (\text{A6})$$

Ohyama *et al.*<sup>36</sup> have proposed an alternate derivation of the LSM based on Fourier-domain analysis of phase shifting with unequal reference phase steps. They have investigated its susceptibility to several noise sources, including random phase-shift errors.

The authors are indebted to Patrick Naulleau and Hector Meddecki for many useful discussions on the development and use of this method. We gratefully acknowledge the support of the Extreme Ultraviolet Limited Liability Company, Intel Corporation, Semiconductor Research Corporation contract 96-LC-460; the Defense Advanced Lithography Program, Defense Advanced Research Projects Agency; and the

Office of Basic Energy Sciences, U.S. Department of Energy under contract DE-AC03-76SF00098.

## References

1. P. Carre, "Installation et utilisation du comparateur photoelectrique et interferential du bureau international des poids et mesures," *Metrologia* **2**, 13–23 (1966).
2. R. Crane, "Interference phase measurement," *Appl. Opt.* **8**, 538–542 (1969).
3. J. H. Bruning, D. R. Herriott, J. E. Gallagher, D. P. Rosenfeld, A. D. White, and D. J. Brangaccio, "Digital wavefront measuring interferometer for testing optical surfaces and lenses," *Appl. Opt.* **13**, 2693–2703 (1974).
4. J. C. Wyant, "Use of an ac heterodyne lateral shear interferometer with real-time wavefront corrections systems (for telescopes)," *Appl. Opt.* **14**, 2622–2626 (1975).
5. J. Schwider, R. Burrow, K. E. Elssner, J. Grzanna, R. Spolaczyk, and K. Merkel, "Digital wavefront measuring interferometry: some systematic error sources," *Appl. Opt.* **22**, 3421–3432 (1983).
6. P. Hariharan, B. F. Oreb, and T. Eiju, "Digital phase-shifting interferometry: a simple error-compensating phase-calculation algorithm," *Appl. Opt.* **26**, 2504–2506 (1987).
7. K. G. Larkin and B. F. Oreb, "Design and assessment of symmetrical phase-shifting algorithms," *J. Opt. Soc. Am. A* **9**, 1740–1748 (1992).
8. J. Schwider, O. Falkenstorfer, H. Schreiber, A. Zoller, and N. Streibel, "New compensating four-phase algorithm for phase-shift interferometry," *Opt. Eng.* **32**, 1883–1885 (1995).
9. Y. Surrel, "Phase stepping: a new self-calibrating algorithm," *Appl. Opt.* **32**, 3598–3600 (1993).
10. K. Hibino, B. F. Oreb, D. I. Farrant, and K. G. Larkin, "Phase shifting for nonsinusoidal waveforms with phase-shift errors," *J. Opt. Soc. Am. A* **12**, 761–768 (1995).
11. Y. Surrel, "Design of algorithms for phase measurements by the use of phase stepping," *Appl. Opt.* **35**, 51–60 (1996).
12. D. W. Phillion, "General methods for generating phase-shifting interferometry algorithms," *Appl. Opt.* **36**, 8098–8115 (1997).
13. J. Schmidt and K. Creath, "Spatial and temporal phase-measurement techniques: a comparison of major error sources in one dimension," in *Interferometry: Techniques and Analysis*, G. M. Brown, O. Y. Kwon, M. Kujawinska, and G. T. Reid, eds., *Proc. SPIE* **1755**, 202–211 (1992).
14. P. J. de Groot, "Derivation of algorithms for phase-shifting interferometry using the concept of a data-sampling window," *Appl. Opt.* **34**, 4723–4730 (1995).
15. J. Wingerden, H. J. Frankena, and C. Smorenburg, "Linear approximation for measurement errors in phase-shifting interferometry," *Appl. Opt.* **30**, 2718–2729 (1991).
16. K. Hibino, "Susceptibility of systematic error-compensating algorithms to random noise in phase-shifting interferometry," *Appl. Opt.* **36**, 2084–2093 (1997).
17. C. P. Brophy, "Effect of intensity error correlation on the computed phase of phase-shifting interferometry," *J. Opt. Soc. Am. A* **7**, 542–551 (1990).
18. C. Rathjen, "Statistical properties of phase-shift algorithms," *J. Opt. Soc. Am. A* **12**, 1997–2008 (1995).
19. K. Kinnstaetter, A. W. Lohmann, J. Schwider, and N. Streibel, "Accuracy of phase shifting interferometry," *Appl. Opt.* **27**, 5082–5089 (1988).
20. G.-S. Han and S.-W. Kim, "Numerical correction of reference phases in phase-shifting interferometry by iterative least-squares fitting," *Appl. Opt.* **33**, 7321–7325 (1994).
21. S.-W. Kim, M.-G. Kang, and G.-S. Han, "Accelerated phase-measuring algorithm of least squares for phase-shifting interferometry," *Opt. Eng.* **36**, 3101–3106 (1997).
22. A. Dobroiu, P. C. Lagofatu, D. Apostol, and V. Damian, "Sta-

- tistical self-calibrating algorithm for three-sample phase-shift interferometry," *Meas. Sci. Technol.* **8**, 738–745 (1997).
23. A. Dobroiu, D. Apostol, V. Nascov, and V. Damian, "Statistical self-calibrating algorithm for phase-shift interferometry based on a smoothness assessment of the intensity offset map," *Meas. Sci. Technol.* **9**, 1451–1455 (1998).
  24. M. Chen, H. Guo, and C. Wei, "Algorithm immune to tilt phase-shifting error for phase-shifting interferometers," *Appl. Opt.* **39**, 3894–3898 (2000).
  25. J. E. Greivenkamp, "Generalized data reduction for heterodyne interferometry," *Opt. Eng.* **23**, 350–352 (1984).
  26. J. E. Greivenkamp and J. H. Bruning, "Phase shifting interferometry," in *Optical Shop Testing*, 2nd ed. D. Malacara, ed. (Wiley, New York, 1992), pp. 522–524.
  27. D. J. Bone, H.-A. Bachor, and R. J. Sandeman, "Fringe-pattern analysis using a 2-D Fourier transform," *Appl. Opt.* **25**, 1653–1660 (1986).
  28. M. Takeda, H. Ina, and S. Kobayashi, "Fourier-transform method of fringe-pattern analysis for computer-based topography and interferometry," *J. Opt. Soc. Am.* **72**, 156–160 (1982).
  29. K. A. Nugent, "Interferogram analysis using an accurate fully automatic algorithm," *Appl. Opt.* **24**, 3101–3105 (1985).
  30. K. A. Goldberg, "EUV interferometry," Ph.D. dissertation (University of California, Berkeley, Berkeley, Calif., 1997).
  31. P. P. Naulleau, K. A. Goldberg, S. H. Lee, C. Chang, D. Atwood, and J. Bokor, "Extreme-ultraviolet phase-shifting point-diffraction interferometer: a wave-front metrology tool with subangstrom reference-wave accuracy," *Appl. Opt.* **38**, 7252–7263 (1999).
  32. D. A. Tichenor, G. D. Kubiak, M. E. Malinowski, R. H. Stulen, S. J. Haney, K. W. Berger, L. A. Brown, W. C. Sweatt, J. E. Bjorkholm, R. R. Freeman, M. D. Himel, A. A. MacDowell, D. M. Tennant, O. R. Wood II, J. Bokor, T. E. Jewell, W. M. Mansfield, W. K. Waskiewicz, D. L. White, and D. L. Windt, "Soft-x-ray projection lithography experiments using Schwarzschild imaging optics," *Appl. Opt.* **32**, 7068–7071 (1993).
  33. K. A. Goldberg, P. Naulleau, and J. Bokor, "EUV interferometric measurements of diffraction-limited optics," *J. Vac. Sci. Technol. B* **17**, 2982–2986 (1999).
  34. P. Hariharan, B. F. Oreb, and T. Eiju, "Digital phase-shifting interferometry: a simple error-compensating phase calculation algorithm," *Appl. Opt.* **26**, 2504–2505 (1987).
  35. P. P. Naulleau and K. A. Goldberg, "Dual-domain point diffraction interferometer," *Appl. Opt.* **38**, 3523–3533 (1999).
  36. N. Ohyama, S. Kinoshita, A. Cornejo-Rodriguez, T. Honda, and J. Tsujiuchi, "Accuracy of phase determination with unequal reference phase shift," *J. Opt. Soc. Am. A* **5**, 2019–2025 (1988).